Mass resolved angular distribution in ^{10}B, ^{12}C, and ^{16}O induced fission of ^{232}Th

Bency John, Aruna Nijasure, and S. K. Kataria
Nuclear Physics Division, Bhabha Atomic Research Centre, Bombay 400085, India

A. Goswami, B. S. Tomar, A. V. R. Reddy, and S. B. Manohar
Radiochemistry Division, Bhabha Atomic Research Centre, Bombay 400085, India
(Received 20 September 1993; revised manuscript received 4 April 1994)

The recoil catcher technique and gamma spectrometric assay of fission products were used to measure angular distribution of 17 fission products in ^{10}B, ^{12}C, and ^{16}O induced fission of ^{232}Th at near barrier energies. The observed mass dependence of anisotropies of fission products in these systems is very different from that of p and α induced fission of ^{232}Th at similar excitation energies. It has been suggested that the difference in the rotational energy for the symmetric and asymmetric modes for large compound nucleus spins could be responsible for the observed variation. No systematic change in the mass dependence of anisotropies across the Bussinaro-Gallone point was observed. For ^{16}O induced fission of ^{232}Th, sharp variation in anisotropies has been observed in the mass region 120–135. This has been attributed to transfer induced fission.

PACS number(s): 25.85.Ge

I. INTRODUCTION

In the statistical theories of fission fragment angular distributions, one relates the observed anisotropies to the shape of the fissioning nucleus at the transition state in the fission process. The earlier studies of the angular distributions have shown that most of the light ion induced fission anisotropies can be understood qualitatively as well as quantitatively when this transition state is identified with the fission saddle point [1]. For the case of heavy ion induced fission involving higher excitation energy and angular momentum, the averaged anisotropies can be understood in many cases only if this transition state lies in between the saddle and scission points [2], implying thereby the role of nonequilibrium degrees of freedom in deciding the mass averaged anisotropies. Since the early days of fission studies on angular distribution, it is an open problem to establish whether there is any correlation between angular and mass distributions. Such a correlation is expected, provided there is some meaningful difference in the distribution of K quantum numbers for different modes of mass division. Further, for high spin systems, if the angular momentum windows for different modes of mass division are different, the angular anisotropy, which is governed by the parameter $p = \langle I^2 \rangle / 4K_0^2$, can be different for these modes.

The radiochemical recoil catcher technique allows measurement of the angular anisotropy of individual fission products, and has been extensively used to study the mass dependence of angular anisotropy in fission. Cohen *et al.* [3] were the first to observe that asymmetric products have higher anisotropy than symmetric products in 22 MeV proton induced fission of ^{232}Th, ^{235}U, ^{238}U, and ^{233}U. The presence of multiple chance fission was a complication in analyzing the data. It has therefore been suggested to carry out such measurements for systems where fission occurs from a single species at a fixed excitation energy. Kapoor *et al.* [4] observed an increase in anisotropy with mass asymmetry in 4.2 MeV neutron induced fission of ^{235}U but no such increase was observed by Vandenbosch, Unik, and Huizenga [5] in the ^{234}U(d,pf) reaction. Recently Wilke *et al.* [6] observed different angular distributions for mass symmetric and mass asymmetric fragments in photon induced fission of ^{236}U with photon end point energy close to the barrier. Correlation between angular anisotropy and fission product mass for light ion induced fission of actinides was also observed by Kudo *et al.* [7] in (p+^{232}Th), Goswami *et al.* [8] in (α+^{233}U), and Datta *et al.* [9] in (α+^{232}Th,^{238}U). All the earlier measurements on proton and alpha induced fission of actinide nuclei show similar trends, that is, increasing anisotropy with increasing mass asymmetry, although with varying slopes. The observed trend of larger anisotropy with increasing mass asymmetry, over and above multichance fission corrections, has been explained assuming that the effective moment of inertia at the transition state decreases with increasing mass asymmetry [9]. Multichance fissions in these cases are expected to change mass asymmetry or peak to valley ratio drastically as compared to first chance fissions, and multichance fission correction of experimental anisotropies for different masses can be ambiguous. Similar experimental studies on anisotropy versus mass asymmetry in heavy ion induced fission are very limited [10–14]. An entrance channel dependence of fragment anisotropies (mass averaged) consistent with the expectations of the "preequilibrium" fission model was observed by Ramamurthy *et al.* [15] in fission induced by ^{10}B, ^{12}C, and ^{16}O ions on thorium and neptunium targets at above barrier energies. An entrance channel dependence of fragment anisotropy versus mass asymmetry in heavy ion induced fission can provide further evidence for preequilibrium fission in terms of correlation between K_0^2 and mass asymmetry.

In the present work, the mass resolved angular distribution in the fission of ^{232}Th induced by ^{10}B, ^{12}C, and ^{16}O projectiles has been studied at above barrier energies. The experimental details are discussed in Sec. II. Results of angular distribution measurements are presented in Sec. III. The observed mass dependence of anisotropies in various systems is discussed in Sec. IV based on angular momentum effects, entrance channel effects, and transfer induced fission effects.

II. EXPERIMENTAL PROCEDURE

Experiments were performed using heavy ion beams from the BARC-TIFR 14 UD pelletron accelerator. The measurements were carried out with ^{16}O beams at 92, 96, and 100 MeV, a ^{12}C beam at 84 MeV, and a ^{10}B beam at 72 MeV on a ^{232}Th target. Fission product anisotropies were measured using the recoil catcher technique for collection of fission fragments, followed by assay of fission product gamma activities. The radiochemical techniques are better in mass resolution but have a limitation on charge determination due to beta decay processes. It is only in the case of shielded nuclei like ^{122,124,126}Sb that a unique determination of mass and charge is possible.

An irradiation chamber of cylindrical geometry having a length of 260 mm and an inner diameter of 146 mm was used. A schematic diagram of the irradiation chamber is shown in Fig. 1. The self-supporting thorium metal target having thickness of 1.3 mg/cm^2 was placed at the center of the chamber at 45° with respect to the beam direction. The beam was collimated using a tantalum collimator having a diameter of 4 mm, placed at the entrance of the chamber. A 5 mm diameter Faraday cup was placed at the chamber exit for current measurement. The distance between the collimator and the Faraday cup was 360 mm. The aluminum catcher foils of 25 μm thickness were mounted in the angular range (θ_{lab}) of 90° to 174°. The foils covered azimuthal angles from 8° to 172° for 90° $< \theta_{lab} <$ 102°, 0° to 180° for 102° $< \theta_{lab} <$ 151°, and 0° to 360° for 162° $< \theta_{lab} <$ 174°, and were divided into eight strips with an average angular width of about 9°. The range of the heaviest fragment under investigation in thorium metal is much larger than the maximum target thickness offered to the emergent fragment at these angles. Measurements in the forward angles were avoided because of the presence of the other reaction products resulting in very complex gamma spectra. In all irradiations the total integrated current was of the order of 0.5–1.0 μA h (particle). After the irradiation, the catcher foils were removed and cut into specified strips. The strips were folded and pressed to the same geometry to have the same efficiency for gamma counting for different strips. The activity of individual fission products was assayed in all the strips over a period of 8–12 days for each irradiation, using an 80 cm^3 HPGe detector coupled to a multichannel analyzer. Energy and photopeak shape calibration of the counting setup was performed using a standard ^{152}Eu source. The resolution of the detector was 2.0 keV at 1332 keV. The strips containing fission product activities were subjected to eight rounds of counting with duration varying from 1 to 15 ksec, starting roughly one hour after the end of the irradiation. The observed gamma spectra were analyzed using the SAMPO code updated for use on a PC-AT with graphic display capabilities. The chosen gamma lines were ascertained to be free from interference from any other gamma lines by checking the half-life of each radionuclide. The measured activities of individual fission products at different time slots were extrapolated to the end time of the irradiation. The mean values of end time activity for various individual products and their standard deviations were used to obtain the mass resolved fragment angular distribution. The nuclear spectroscopic data used for the present work were taken from Ref. [16].

The activities in various strips, corrected for their dif-

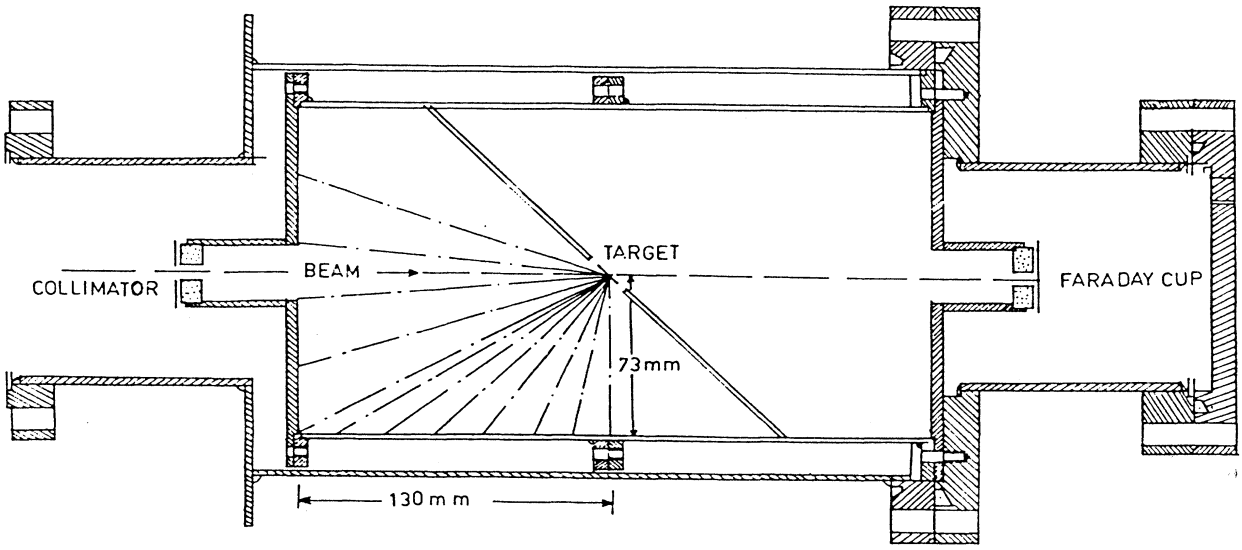

FIG. 1. Schematic diagram of the irradiation chamber.

ference in azimuthal angle, are proportional to the intensity of fission products emitted at $\theta_{\rm lab}$ at which the strips were located during the bombardment. From the activity data the laboratory angular distribution for the ith mass was arrived at using the following equation:

$$W^i(\theta_{\rm lab}) = A^i/\pi[\cos(\theta_{1\,\rm lab}) - \cos(\theta_{2\,\rm lab})]\ , \qquad (1)$$

where A^i is the fission product activity of the ith mass and $\theta_{1\,\rm lab}$ and $\theta_{2\,\rm lab}$ correspond to two extreme angles for each strip such that $\pi[\cos(\theta_{1\,\rm lab}) - \cos(\theta_{2\,\rm lab})]$ is the solid angle of the strip. The laboratory angular distributions were converted to the center of mass system by assuming full momentum transfer of the incident ion to the compound nucleus. The average total kinetic energy (TKE) release for the systems was taken from Viola, Kwiatowski, and Walker systematics [17]. The variation of TKE with mass ratio was calculated from the Coulomb force between complementary mass fragments. The average kinetic energy of a particular mass fragment was obtained using these systematics. A Monte Carlo simulation study showed that, for any reasonable kinetic energy distribution of a particular mass split, the trans-

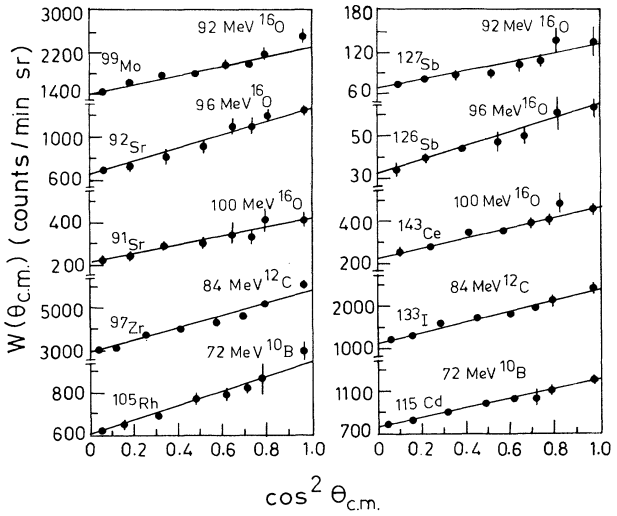

FIG. 2. Center of mass angular distributions for a few fission products in the fission of ^{232}Th induced by projectiles as indicated. The solid lines are obtained by least squares fitting.

TABLE I. Angular anisotropies of fission products.

Nuclide	^{16}O+^{232}Th 100 MeV	^{16}O+^{232}Th 96 MeV	^{16}O+^{232}Th 92 MeV	^{12}C+^{232}Th 84 MeV	^{10}B+^{232}Th 72 MeV
^{91}Sr	1.94	1.99	1.40	1.97	1.51
	(0.13)	(0.10)	(0.20)	(0.16)	(0.05)
^{92}Sr	1.97	1.87		1.96	1.51
	(0.09)	(0.03)		(0.12)	(0.09)
^{97}Zr	1.99	1.95	1.55	1.97	1.47
	(0.14)	(0.04)	(0.13)	(0.13)	(0.05)
^{99}Mo	1.99	2.02	1.60	1.99	1.58
	(0.09)	(0.05)	(0.11)	(0.13)	(0.05)
^{103}Ru	2.08	2.03	1.66	1.99	1.56
	(0.09)	(0.08)	(0.08)	(0.12)	(0.07)
^{105}Rh	2.12	2.05	1.71	2.07	1.54
	(0.09)	(0.04)	(0.06)	(0.17)	(0.05)
^{112}Pd	2.04	2.03	1.68	2.02	1.55
	(0.10)	(0.09)	(0.09)	(0.14)	(0.02)
^{115}Cd	2.04	2.03	1.61	2.00	1.59
	(0.10)	(0.03)	(0.11)	(0.11)	(0.02)
^{122}Sb	2.54	2.14	1.74	2.0	1.62
	(0.20)	(0.04)	(0.15)	(0.13)	(0.07)
^{126}Sb	2.17	2.16	1.82	1.83	1.62
	(0.20)	(0.09)	(0.10)	(0.05)	(0.07)
^{127}Sb	2.34	2.11	1.90	2.14	1.60
	(0.19)	(0.03)	(0.11)	(0.11)	(0.06)
^{130}I	2.21	2.12	1.65	2.00	1.59
	(0.11)	(0.06)	(0.10)	(0.10)	(0.03)
^{131}I	1.98	2.02	1.55	2.05	1.58
	(0.10)	(0.08)	(0.05)	(0.13)	(0.04)
^{132}Te	1.82	1.90	1.40	1.98	1.54
	(0.17)	(0.13)	(0.10)	(0.17)	(0.03)
^{133}I	1.90	1.84	1.63	2.03	1.53
	(0.15)	(0.05)	(0.16)	(0.16)	(0.04)
^{141}Ce	2.08	1.74	1.59	2.29	1.47
	(0.07)	(0.14)	(0.17)	(0.20)	(0.03)
^{143}Ce	2.11	1.96	1.66	2.20	1.63
	(0.08)	(0.08)	(0.07)	(0.15)	(0.03)

formation factor is nearly identical to the one obtained using average kinetic energy alone within 0.5%. However, this transformation factor depends sensitively on fission fragment masses and associated average kinetic energies and, therefore, the derived anisotropies depend on the systematics of TKE with mass ratio.

The observed angular distributions $W(\theta_{\text{c.m.}})$ for a few fragment masses are plotted against $\cos^2\theta_{\text{c.m.}}$ as shown in Fig. 2. As seen from the figure, the observed angular distributions can be well represented by the standard expression $W(\theta) = a + b\cos^2\theta$. Using the method of weighted least squares regression, the experimental data were fitted by the above expression and values of the anisotropy were obtained. It was observed that the inclusion of higher order terms did not give a better fit.

III. RESULTS

The anisotropy values for 17 fission product masses measured in this work are given in Table I for all the systems. The statistical errors on the anisotropy values are shown in the parentheses.

Figure 3 shows the plot of anisotropy versus fission product mass for the $^{12}C+^{232}Th$ system at $E_{\text{lab}} = 84$ MeV and the $^{10}B+^{232}Th$ system at $E_{\text{lab}} = 72$ MeV. Angular anisotropies for these systems do not appear to depend on the mass asymmetry significantly as can be seen from the figure. The solid lines are drawn through the points to guide the eye.

Figure 4 shows the plot of anisotropy versus fission product mass for the $^{16}O+^{232}Th$ system at $E_{\text{lab}} = 92$, 96, and 100 MeV. As can be seen from the figure, the increase in the average anisotropy from 92 to 96 MeV is rather large as compared to its change from 96 to 100 MeV for all the product masses. It is also seen that there is a sharp variation in anisotropy in the mass region 120–135 at all three energies. If this local variation is averaged, then there seems to be a mass dependence of anisotropy with the symmetric products tending to have higher anisotropy than the asymmetric products.

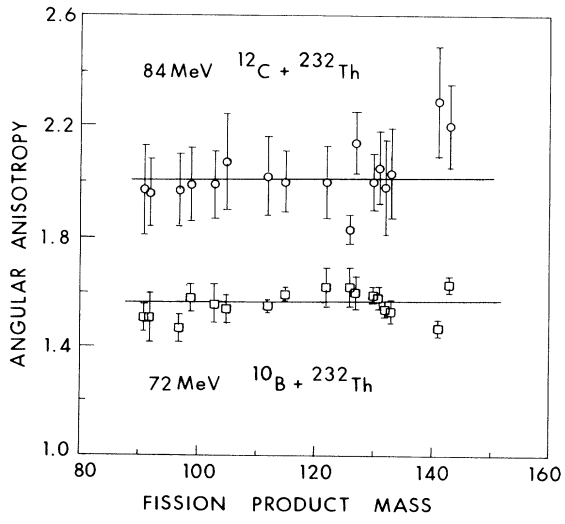

FIG. 3. Plot of angular anisotropy versus fission product mass for 84 MeV ^{12}C and 72 MeV ^{10}B induced fission of ^{232}Th. The solid lines are merely to guide the eye.

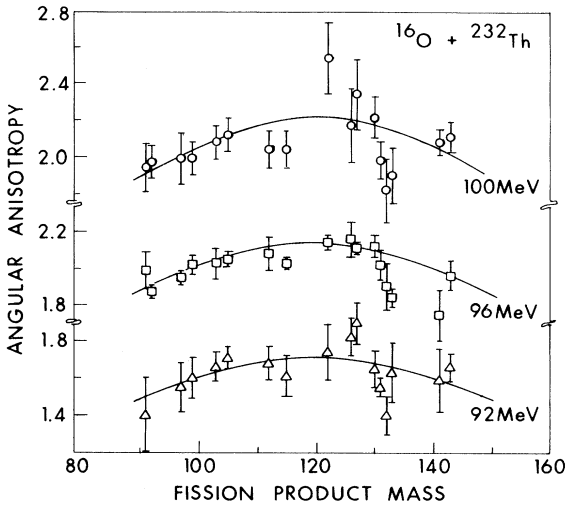

FIG. 4. Plot of angular anisotropy versus fission product mass for ^{16}O induced fission of ^{232}Th at $E_{\text{lab}} = 92$, 96, and 100 MeV. The solid curves are merely to guide the eye.

Because of the large error bars on the anisotropy, particularly at 92 and 100 MeV, we thought that a better picture of overall mass dependence of anisotropy would emerge if normalized angular distributions of individual fission products are grouped together into different mass bins representing varying mass asymmetry and angular anisotropies extracted for these mass bins. Such averaging would also smooth the local fluctuation in anisotropy. Such plots of angular distribution are shown in Fig. 5 for the 100 MeV $^{16}O+^{232}Th$ and 72 MeV $^{10}B+^{232}Th$ systems where a bin of 8 mass units was chosen. Products that are equal mass units away from symmetric masses on either side were grouped together. Approximate values of symmetric masses, expected from the systematics of prefission and postfission neutron multiplicities [18], were used. The symmetric masses thus calculated were in agreement with the experimental fission product yield data [19,20]. The anisotropies corresponding to each mass grouping were obtained by fitting the data to the standard expression using the method of least squares regression and the values are given in Table II. The statistical errors on the anisotropy values are shown in the parentheses. The corresponding nuclides in each group are also given in this table. It is seen that, for the $^{12}C+^{232}Th$ and $^{10}B+^{232}Th$ systems, there is no variation of anisotropy, while for the $^{16}O+^{232}Th$ system, anisotropy decreases with mass asymmetry at all three energies. A similar trend has also been observed for the $^{16}O+^{238}U$ system at 101 MeV [10].

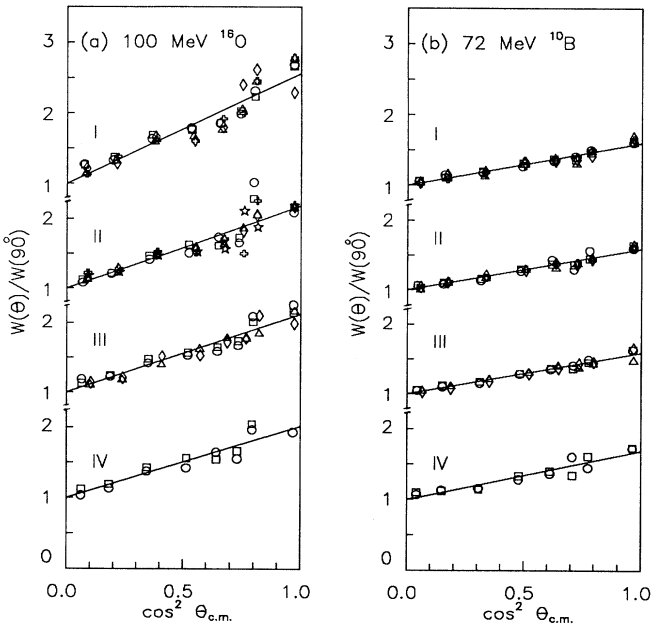

FIG. 5. Center of mass angular distributions for (a) 100 MeV ^{16}O and (b) 72 MeV ^{10}B induced fission of ^{232}Th for four mass asymmetry groups. Symbols used for different nuclides in each group are group I: ^{112}Pd (circle), ^{115}Cd (square), ^{122}Sb (triangle), ^{126}Sb (diamond), ^{127}Sb (cross); group II: ^{103}Ru (circle), ^{105}Rh (square), ^{130}I (triangle), ^{131}I (diamond), ^{132}Te (cross), ^{133}I (star); group III: ^{97}Zr (circle), ^{99}Mo (square), ^{141}Ce (triangle), ^{143}Ce (diamond); group IV: ^{91}Sr (circle), ^{92}Sr (square). The solid lines are obtained by least squares fitting.

IV. DISCUSSION

A. Angular momentum effects

The mass dependence of anisotropy shows a qualitative change in average trends as one goes from light ion to heavy ion induced fission of ^{232}Th. For p+^{232}Th and α+^{232}Th systems anisotropy increases from symmetric to asymmetric mass division. The average trends of anisotropy versus mass asymmetry for the ^{12}C+^{232}Th and ^{10}B+^{232}Th systems measured in the present work do not show significant dependence on mass asymmetry. The data for the ^{16}O+^{232}Th system indicate larger anisotropy for symmetric mass division as compared to asymmetric mass division, more so at the highest energy of 100 MeV.

In low energy fission as well as light ion induced fission of actinides the role of shell structure effects in producing a double humped mass distribution has been well studied. The characteristic feature of the mass distribution in heavy ion induced fission in the actinide region is that it is a broad symmetric distribution and is quite different from the asymmetric distribution of low energy fission. No calculation of the mass distribution in heavy ion induced fission of actinides based on vanishing shell effects with increase in excitation energy and the effect of a large range of angular momenta have been reported so far. It is well known that fission barriers decrease as a function of compound nucleus spin I. Further, the moment of inertia of the symmetric saddle (scission) point is greater than that for the asymmetric saddle (scission) point. Therefore, for high angular momentum states where the rotational energy correction is comparable to the fission barrier $B_f(I=0)$, the asymmetric mass division is likely to be suppressed depending on the magnitude of the shell correction energies. In other words, for high angular momentum fission events, the mass yield at symmetry increases and the final mass distribution becomes a very broad symmetric distribution as is seen experimentally [18–20]. The rms value of angular momentum $\langle I^2\rangle$ and its projection along the fission axis $\langle K^2\rangle$ for the fission channel in these cases will depend on the mass asymmetry.

An estimate of the anisotropy parameter $p = \langle I^2\rangle/4\langle K^2\rangle$ for symmetric and asymmetric modes of mass division has been made for a few systems, taking into account the effect of rotational energy on fission width Γ_f for the two modes. The $\langle I^2\rangle$ and the $\langle K^2\rangle$ were calculated for the two modes in the following way:

$$\langle I^2\rangle_{\rm sym} = \frac{\sum_{I=0}^{\infty}\sum_{K=-I}^{I} I^2\sigma_I\Gamma^r_{f\,\rm sym}(I,K)}{\sum_{I=0}^{\infty}\sum_{K=-I}^{I}\sigma_I\Gamma^r_{f\,\rm sym}(I,K)}, \qquad (2)$$

$$\langle K^2\rangle_{\rm sym} = \frac{\sum_{I=0}^{\infty}\sum_{K=-I}^{I} K^2\sigma_I\Gamma^r_{f\,\rm sym}(I,K)}{\sum_{I=0}^{\infty}\sum_{K=-I}^{I}\sigma_I\Gamma^r_{f\,\rm sym}(I,K)}, \qquad (3)$$

TABLE II. Angular anisotropies of different mass groupings.

	Nuclides	^{16}O+^{232}Th 100 MeV	^{16}O+^{232}Th 96 MeV	^{16}O+^{232}Th 92 MeV	^{12}C+^{232}Th 84 MeV	^{10}B+^{232}Th 72 MeV
Group I	^{112}Pd, ^{115}Cd, ^{122}Sb	2.57	2.19	1.79	2.03	1.60
	^{126}Sb, ^{127}Sb	(0.18)	(0.063)	(0.09)	(0.05)	(0.03)
Group II	^{103}Ru, ^{105}Rh, ^{130}I	2.18	2.07	1.53	2.11	1.59
	^{131}I, ^{132}Te, ^{133}I	(0.13)	(0.08)	(0.07)	(0.06)	(0.03)
Group III	^{97}Zr, ^{99}Mo, ^{141}Ce	2.12	2.02	1.57	2.16	1.59
	^{143}Ce	(0.10)	(0.08)	(0.08)	(0.08)	(0.03)
Group IV	^{91}Sr, ^{92}Sr	2.01	2.14	1.52	2.12	1.69
		(0.17)	(0.10)	(0.26)	(0.13)	(0.09)

$$\langle I^2\rangle_{\rm asym} = \frac{\sum_{I=0}^{\infty}\sum_{K=-I}^{I} I^2\sigma_I\Gamma^r_{f\,\rm asym}(I,K)}{\sum_{I=0}^{\infty}\sum_{K=-I}^{I}\sigma_I\Gamma^r_{f\,\rm asym}(I,K)}\,, \tag{4}$$

$$\langle K^2\rangle_{\rm asym} = \frac{\sum_{I=0}^{\infty}\sum_{K=-I}^{I} K^2\sigma_I\Gamma^r_{f\,\rm asym}(I,K)}{\sum_{I=0}^{\infty}\sum_{K=-I}^{I}\sigma_I\Gamma^r_{f\,\rm asym}(I,K)}\,, \tag{5}$$

where σ_I is the partial cross section for the formation of compound nucleus with spin I and $\Gamma^r_{f\,\rm sym}(I,K)$ and $\Gamma^r_{f\,\rm asym}(I,K)$ are the relative fission widths for symmetric and asymmetric modes, respectively, calculated using the following equations:

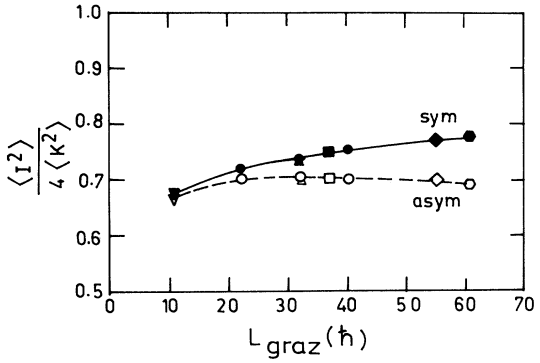

FIG. 6. Plot of anisotropy parameter $p = \langle I^2\rangle/4\langle K^2\rangle$ versus $L_{\rm graz}$. The closed symbols are for symmetric mode and open symbols are for asymmetric mode of mass division. The symbols used for different systems are 92, 96, and 100 MeV ^{16}O+^{232}Th (circle), 30 MeV α+^{232}Th (inverted triangle), 72 MeV ^{10}B+^{232}Th (triangle), 84 MeV ^{12}C+^{232}Th (square), 120 MeV ^{12}C+^{238}U (diamond), and 135 MeV ^{16}O+^{238}U (hexagon). The lines are merely to guide the eye.

$$\Gamma^r_{f\,\rm sym}(I,K) = \frac{\Gamma_f(E^* - B_f - E_{R\,\rm sym}(I,K))}{\Gamma_f(E^* - B_f - E_{R\,\rm sym}(I,K)) + \Gamma_f(E^* - B_f - E_{R\,\rm asym}(I,K))}\,, \tag{6}$$

$$\Gamma^r_{f\,\rm asym}(I,K) = \frac{\Gamma_f(E^* - B_f - E_{R\,\rm asym}(I,K))}{\Gamma_f(E^* - B_f - E_{R\,\rm sym}(I,K)) + \Gamma_f(E^* - B_f - E_{R\,\rm asym}(I,K))}\,, \tag{7}$$

where E^* is the excitation energy of the compound nucleus, B_f is the fission barrier calculated using the liquid drop model, and $E_{R\,\rm sym}$ and $E_{R\,\rm asym}$ are the rotational energies calculated for symmetric ($A_H/A_L \approx 1$) and asymmetric ($A_H/A_L \approx 1.4$) saddle point shapes using (c,h,α) parametrization [21]. We have used a single set of (c,h,α) parameters suitable for actinides, for all the nuclei considered. Figure 6 shows the plot of the anisotropy parameter p for symmetric and asymmetric modes versus fusion $L_{\rm graz}$ parameter. For light ion induced fission, where the magnitude of rotational energy is small, the anisotropy parameters for the two modes are nearly same. Experimentally observed anisotropy for the two modes can be explained only by the variation of K_0^2 with mass asymmetry, originating from shell effects as shown by [9]. For heavy ion induced fission, where there is a reduction in shell effects and an increase in rotational energy, the anisotropy parameter for the symmetric mode is larger than for the asymmetric mode, as can be seen from Fig. 6. The resultant anisotropy for symmetric mass division will increase with $L_{\rm graz}$ more rapidly than for asymmetric mass division. For ^{10}B, ^{12}C, and ^{16}O induced fission of thorium in the present energy range, the relative increase in anisotropy for symmetric fission is about 5–7 %. Multichance fission corrections for these cases could not be performed because of the lack of knowledge of the prescission neutron multiplicity as a function of fragment mass.

B. Entrance channel dependence

The compound nucleus fissility and entrance channel mass asymmetry parameter $\alpha = (A_T - A_P)/(A_T + A_P)$ where A_T and A_P are target and projectile mass numbers for the systems studied are listed in Table III. For ^{10}B+^{232}Th and ^{12}C+^{232}Th systems, the mass asymmetry parameter is greater than $\alpha_{\rm BG}$, the Businaro-Gallone critical asymmetry value [22], whereas for the ^{16}O+^{232}Th system α is less than $\alpha_{\rm BG}$. Table III also lists mass averaged anisotropy values at various bombarding energies calculated using the standard saddle point model (SSM) and the measured values for these systems. The measured values given are average values over all masses without any weight factor for mass yields. For the case of the ^{16}O+^{232}Th system, the measured value of anisotropy is significantly higher than the statistical model value, as also seen earlier [15,23].

The observed high anisotropy for the ^{16}O+^{232}Th system cannot be explained by the transfer induced fission mechanism alone, as shown by Lestone *et al.* [24]. The ^{16}O+^{232}Th system has higher prescission neutron multiplicity compared to other systems, as shown by Saxena *et al.* [25]. This means fission is more delayed in this case. This dynamical delay can also be responsible for an evolution of K distribution beyond the saddle point thus increasing the value of the anisotropy compared to the standard saddle point model [2]. If the dynamical delay

TABLE III. Relevant parameters for the systems studied.

System	^{16}O+^{232}Th	^{16}O+^{232}Th	^{16}O+^{232}Th	^{12}C+^{232}Th	^{10}B+^{232}Th
Bombarding energy (MeV)	100	96	92	84	72
Entrance channel mass asymmetry α	0.871	0.871	0.871	0.902	0.971
Compound nucleus fissility	0.8254	0.8254	0.8254	0.8073	0.798
Excitation energy (MeV)	57.1	53.3	49.5	56.9	61.2
L_{graz} ($\hbar$)	40	32	22	37	32
Anisotropy (calculated)	1.80	1.66	1.53	1.90	1.67
Anisotropy (experiment)	2.1	2.0	1.6	2.0	1.56

is more for symmetric masses compared to asymmetric masses [26], correspondingly symmetric masses will show higher anisotropy compared to asymmetric ones.

The observed mass dependence of anisotropy for ^{16}O+^{232}Th is similar to that for ^{16}O+^{238}U within the experimental errors [10], but the latter system shows agreement when the average value is compared with the statistical model value [23]. The ^{10}B+^{232}Th and ^{12}C+^{232}Th systems show no mass dependence of anisotropy within the experimental errors.

C. Effect of transfer induced fission

The sharp variation in anisotropy in the mass region 120–135 and its absence on the lighter side of the symmetric mass in the ^{16}O+^{232}Th system show that the radiochemically determined value of anisotropy of a fission product can deviate from the average value for that mass number. This can happen when the yield of the fission product in question is the true independent yield, not the cumulative yield following the beta decay of the precursors. Many isotopes of antimony, tellurium, and iodine fall in this category. Recently [27], variation of yields of these isotopes as a function of their neutron to proton ratio in ^{12}C induced fission of ^{233,235,238}U has been conveniently used to identify whether a given fission product originates from fission following complete fusion (CF) or from fission following transfer of a nucleon or a cluster of nucleons from projectile to target. Using charge distribution systematics, it has been shown that, for a given fission product charge, as one goes from neutron deficient isotope to progressively more neutron rich isotope their source of formation changes from CF to transfer induced fission. This is expected as transfer induced fission will occur from an intermediate nucleus with lower excitation energy, and hence final products will form with lesser number of evaporated neutrons [28]. On the same grounds, it can be expected that angular anisotropies of neutron rich products formed from transfer induced fission should carry the signature of the process. This has already been revealed in the work of Todd *et al.* [12], where a plot of angular anisotropies of Sb, Te, and I isotopes versus N/Z ratio shows lower anisotropy for neutron rich products which are likely to originate from an intermediate nucleus with lower excitation energy.

It is to be noticed from the present data that the sharp variation in anisotropy in this mass region is typical of the ^{16}O+^{232}Th system and is absent in the ^{10}B+^{232}Th and ^{12}C+^{232}Th systems. In Fig. 7 we have plotted the angular anisotropies of ^{122,126}Sb, ^{132}Te, and ^{130,131,133}I as a function of their A/Z ratio for all the systems studied in the present work. A trend of decreasing anisotropy with the increase in A/Z ratio is clearly seen for the ^{16}O+^{232}Th system and this trend is absent in the ^{12}C+^{232}Th and ^{10}B+^{232}Th systems. This suggests that transfer induced fission is significant for the former

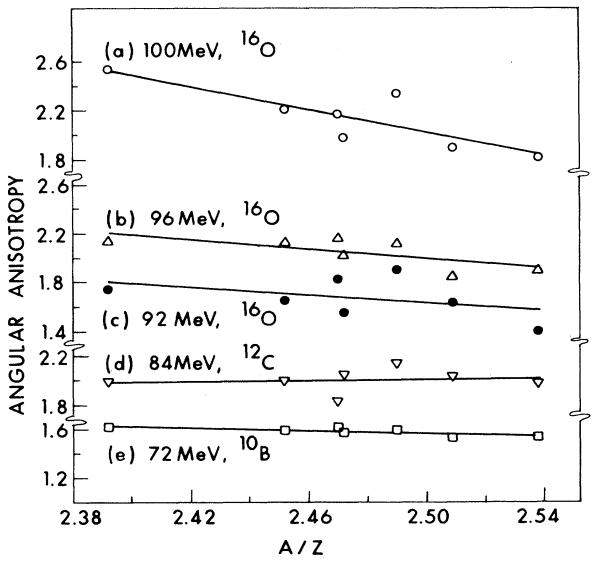

FIG. 7. Plot of angular anisotropy versus A/Z ratio for the fission products ^{122,126}Sb, ^{132}Te, and ^{130,131,133}I for various systems as indicated. The solid lines are obtained by least squares fitting.

system and is insignificant for the latter two systems.

The assumption of full momentum transfer while transforming the laboratory angular distribution to the center of mass system is not strictly valid for these fission products originating in transfer induced fission. However, this assumption can lead only to an underestimation of the isotopic variation.

V. SUMMARY

Mass resolved fission fragment angular distribution measurements have been carried out with ^{16}O beams at 92, 96, and 100 MeV, a ^{12}C beam at 84 MeV, and a ^{10}B beam at 72 MeV incident on a ^{232}Th target. Fission product anisotropies were measured using the recoil catcher technique followed by assay of their gamma activities. The observed mass dependence of anisotropy is different from that for light ion induced fission of thorium. It has been suggested that this could arise due to difference in rotational energy for symmetric and asymmetric modes of mass division of fissioning nuclei.

ACKNOWLEDGMENTS

We are thankful to the operating staff of the Pelletron accelerator facility at TIFR for making available the required beams. We thank Dr. S. S. Kapoor, Dr. V. S. Ramamurthy, and Dr. R. H. Iyer for their encouragement and many valuable suggestions during the course of this work. We thank P. P. Burte for his valuable help during the course of the experiment and B. Singh for providing us with the PC version of the SAMPO program.

[1] I. Halpern and V. M. Strutinsky, in *Proceedings of the Second United Nation International Conference on Peaceful Uses of Atomic Energy*, Geneva, 1958 (United Nations, New York, 1958), Vol. 15, p. 408.

[2] R. Freifelder, M. Prakash, and J. M. Alexander, Phys. Rep. **133**, 315 (1986).

[3] B. L. Cohen, B. L. Ferrel-Bryan, D. J. Coombe, and M. K. Hullings, Phys. Rev. **98**, 685 (1955).

[4] S. S. Kapoor, D. M. Nadkarni, R. Ramanna, and P. N. Rama Rao, Phys. Rev. **137**, B511 (1965).

[5] R. Vandenbosch, J. P. Unik, and J. R. Huizenga, in *Proceedings of IAEA Symposium on Physics and Chemistry of Fission*, Salzburg, 1965 (IAEA, Vienna, 1965), Vol. 1, p. 547.

[6] W. Wilke, R. D. Heil, U. Kneissel, U. Seemann, F. Stepier, H. Stroher, and T. Weber, Phys. Lett. B **207**, 385 (1988).

[7] H. Kudo, Y. Nagame, H. Nakahara, K. Miyano, and I. Kohno, Phys. Rev. C **25**, 909 (1982).

[8] A. Goswami, S. B. Manohar, S. K. Das, A. V. R. Reddy, B. S. Tomar, and Satya Prakash, Z. Phys. A **342**, 299 (1992).

[9] T. Datta, S. P. Dange, H. Naik, and S. B. Manohar, Phys. Rev. C **48**, 221 (1993).

[10] D. J. Parker, J. J. Hogan, and J. Asher, Z. Phys. A **336**, 411 (1991).

[11] J. J. Hogan, D. J. Parker, and J. Asher, Z. Phys. A **338**, 325 (1991).

[12] J. R. D. Todd, A. R. Wolf, J. J. Hogan, and D. J. Parker, J. Phys. G **19**, 187 (1993).

[13] W. Q. Shen, J. Albinski, A. Gobbi, S. Gralla, K. D. Hildenbrand, N. Herrmann, J. Kuzminski, W. F. J. Muller, H. Stelzer, J. Toke, B. B. Back, S. Bjornholm, and S. P. Sorensen, Phys. Rev. C **36**, 115 (1987).

[14] J. Toke, R. Bock, G. X. Dai, A. Gobbi, S. Gralla, K. D. Hildenbrand, J. Kuzminski, W. F. G. Muller, A. Olmi, W. Reisdorf, S. Bjornholm, and B. B. Back, Phys. Lett. **142B**, 258 (1984).

[15] V. S. Ramamurthy, S. S. Kapoor, R. K. Choudhury, A. Saxena, D. M. Nadkarni, A. K. Mohanty, B. K. Nayak, S. V. S. Sastry, S. Kailas, A. Chatterjee, P. Singh, and A. Navin, Phys. Rev. Lett. **65**, 25 (1990).

[16] U. Reus and W. Westmeier, At. Data Nucl. Data Tables **29**, 1 (1983).

[17] V. E. Viola, K. Kwiatowski, and M. Walker, Phys. Rev. C **31**, 1550 (1985).

[18] U. Schroder and J. R. Huizenga, Nucl. Phys. **A502**, 473 (1989).

[19] S. B. Manohar, A. Goswami, A. V. R. Reddy, B. S. Tomar, P. P. Burte, and Satya Prakash, Radiochim. Acta **56**, 69 (1992).

[20] A. Goswami, A. V. R. Reddy, B. S. Tomar, P. P. Burte, S. B. Manohar, and Bency John, Radiochim. Acta **62**, 173 (1994).

[21] M. Brack, Jens Damgaard, A. S. Jensen, H. C. Pauli, V. M. Strutinski, and C. Y. Wong, Rev. Mod. Phys. **144**, 320 (1972).

[22] M. Abe, KEK Report No. 86-26, KEK, TH-28, 1986.

[23] B. B. Back, R. B. Betts, J. E. Gindler, B. D. Wilkins, S. Saini, M. B. Tsang, C. K. Gelbke, W. J. Lynch, M. A. McMahan, and P. A. Baisden, Phys. Rev. C **32**, 195 (1985).

[24] J. P. Lestone, J. R. Leigh, J. O. Newton, and J. X. Wei, Nucl. Phys. **A509**, 178 (1990).

[25] A. Saxena, A. Chatterjee, R. K. Choudhury, S. S. Kapoor, and D. M. Nadkarni, Phys. Rev. C **49**, 932 (1994).

[26] D. J. Hinde, D. Hilscher, H. Rossner, B. Gebauor, M. Lehmann, and M. Wilpert, Phys. Rev. C **45**, 1229 (1992).

[27] M. C. Duh, H. Baba, N. Takahashi, A. Lokoyama, T. Sito, S. Baba, and K. Hata, Nucl. Phys. **A550**, 281 (1992).

[28] A. Pagano, S. Aiello, E. De Filippo, G. Lanzano, S. Lo-Nigro, C. Milone, G. Blancato, G. Di Marco, and M. C. Mermaz, Phys. Rev. C **47**, 1170 (1993).